JOURNAL OF GEOPHYSICAL RESEARCH, VOL. 115, A06314, doi:10.1029/2009JA014563, 2010

Ion transport in Titan's upper atmosphere

J. Cui,[1] M. Galand,[1] R. V. Yelle,[2] J.-E. Wahlund,[3] K. Ågren,[3] J. H. Waite Jr.,[4] and M. K. Dougherty[1]

Received 13 June 2009; revised 13 December 2009; accepted 5 January 2010; published 23 June 2010.

[1] Based on a combined Cassini data set including Ion Neutral Mass Spectrometer, Radio Plasma Wave Science, and Magnetometer measurements made during nine close encounters of the Cassini spacecraft with Titan, we investigate the electron (or total ion) distribution in the upper ionosphere of the satellite between 1250 and 1600 km. A comparison of the measured electron distribution with that in diffusive equilibrium suggests global ion escape from Titan with a total ion loss rate of ~$(1.7 \pm 0.4) \times 10^{25}$ s^{-1}. Significant diurnal variation in ion transport is implied by the data, characterized by ion outflow at the dayside and ion inflow at the nightside, especially below ~1400 km. This is interpreted as a result of day-to-night ion transport, with a horizontal transport rate estimated to be ~$(1.4 \pm 0.5) \times 10^{24}$ s^{-1}. Such an ion flow is likely to be an important source for Titan's nightside ionosphere, as proposed in *Cui et al.* [2009a].

Citation: Cui, J., M. Galand, R. V. Yelle, J.-E. Wahlund, K. Ågren, J. H. Waite Jr., and M. K. Dougherty (2010), Ion transport in Titan's upper atmosphere, *J. Geophys. Res.*, *115*, A06314, doi:10.1029/2009JA014563.

1. Introduction

[2] The Voyager 1 radio occultation experiment revealed the presence of a substantial ionosphere on Titan [*Bird et al.*, 1997]. This discovery was later confirmed by multi-instrumental observations made during the Titan flybys of the Cassini spacecraft [e.g., *Wahlund et al.*, 2005; *Cravens et al.*, 2005, 2006; *Kliore et al.*, 2008]. Pre-Cassini investigations considered both photoionization by solar radiation and impact ionization by magnetospheric electrons as the ionizing sources for Titan's upper ionosphere [e.g., *Ip*, 1990; *Gan et al.*, 1992; *Keller et al.*, 1992; *Galand et al.*, 1999], but the relative importance of the two sources was not well constrained until recently. The complex interaction between Titan's upper atmosphere and Saturn's magnetosphere, which varies both over the satellite and with the satellite's position in the magnetosphere, made resolution of this question difficult on the basis of Voyager data and theoretical considerations alone.

[3] Cassini data has shown quite definitively that solar radiation is the dominant ionization source for the dayside ionosphere. Ionospheric models for the dayside require no additional ionization sources beyond solar radiation to explain the ion and electron densities observed by Cassini instruments [e.g., *Cravens et al.*, 2005]. Analysis of the large Radio and Plasma Wave Science (RPWS) data set shows a clear correlation of the peak altitude and density of the observed electron distribution with solar zenith angle [*Ågren et al.*, 2009]. Calculations of the electron temperature on the dayside based on solar input alone are in good agreement with observed electron temperatures [*Galand et al.*, 2006]. Finally, the dominance of solar input is also supported by observations of Titan's airglow emissions [*Ajello et al.*, 2007].

[4] On the contrary, the nightside ionosphere of Titan has been suggested to be produced by electron precipitation from Saturn's magnetosphere [e.g., *Ågren et al.*, 2007; *Cravens et al.*, 2008], perhaps not surprising in view of its long rotation period of ~16 days. This is supported by the nightside ionospheric measurements made during the T5 flyby, for which the Ion Neutral Mass Spectrometer (INMS) ion density of CH_5^+ is found to be correlated with the Cassini Plasma Spectrometer (CAPS) electron flux [*Cravens et al.*, 2008]. However, based on an analysis of the distinct diurnal variations of short-lived and long-lived ions in Titan's ionosphere, *Cui et al.* [2009a] suggested instead that the primary ion source for the nightside of Titan is chemical survival of dayside ions. Such a scenario is supported by the apparent correlation between the day-to-night ion density ratios measured by the INMS and the associated ion lifetimes estimated from photochemical models [*Cui et al.*, 2009a]. Similar effect of day-to-night transport as the source for the nightside ionosphere has been extensively discussed for other planets, such as Venus [e.g., *Whitten et al.*, 1982; *Cravens et al.*, 1983; *Brannon et al.*, 1993; *Tanaka and Murawski*, 1997]. It is worth mentioning that the nature of day-to-night ion transport in Titan's upper atmosphere is to be distinguished from that on Venus, for which the ion transport is driven by thermal winds blowing from the dayside to the nightside through both terminators and the ion distribution is roughly symmetric between the dawn and dusk. On the other hand, the day-to-night ion transport on

[1]Space and Atmospheric Physics Group, Department of Physics, Imperial College London, London, UK.
[2]Lunar and Planetary Laboratory, University of Arizona, Tucson, Arizona, USA.
[3]Swedish Institute of Space Physics, Uppsala, Sweden.
[4]Southwest Research Institute, San Antonio, Texas, USA.

0148-0227/10/2009JA014563

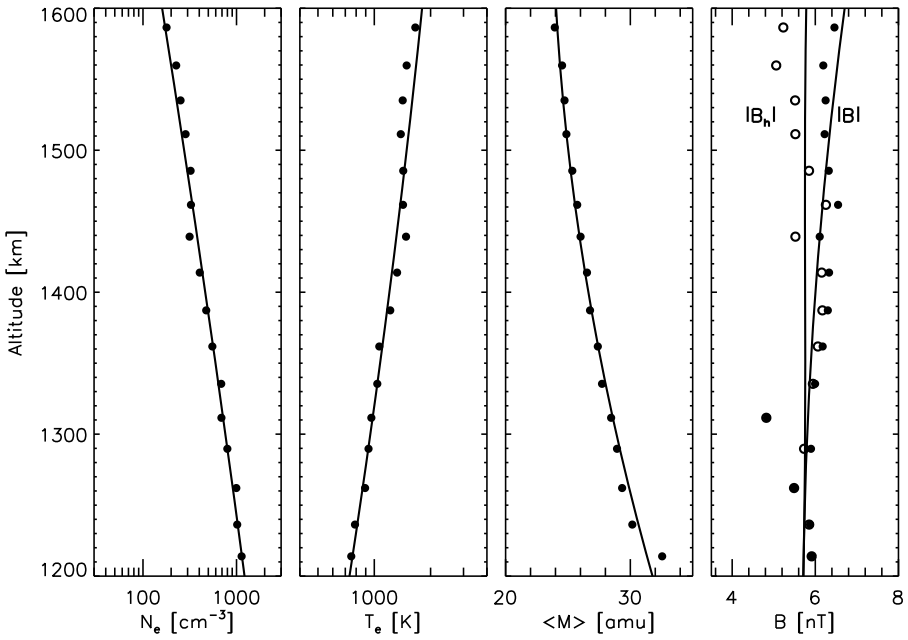

Figure 1. The altitude profiles of various parameters, including electron (or total ion) density, electron temperature, mean ion mass and magnetic field strength, obtained from the INMS, RPWS, and MAG measurements averaged over all flybys in our sample. The magnitudes of both the total magnetic field, $|B|$ (solid circles) and its horizontal component, $|B_h|$ (open circles) are presented. The solid lines give the empirical fits to different parameters.

Titan could be either associated with solid-body rotation of the satellite or enhanced by superrotating neutral winds [e.g., *Müller-Wodarg et al.*, 2000, 2008]. In such cases, the ion/electron density at dusk is expected to be higher than that at dawn since ions observed at dawn spend more time in darkness. Such a dawn-dusk asymmetry on Titan has already been revealed by the Cassini data [*Cui et al.*, 2009a]. A more detailed comparison between the day-to-night ion transport and magnetospheric electron precipitation as two independent sources for Titan's nightside ionosphere has been presented in *Cui et al.* [2009a].

[5] The survival of dayside ions well into the nightside implies the presence of horizontal ion flow on Titan, which may cause departure in the observed ion density profile from that in diffusive equilibrium. Such a departure may also be driven by ion escape from Titan, which has been both estimated from Cassini observations [e.g., *Wahlund et al.*, 2005] and predicted by magnetohydrodynamics (MHD) or hybrid simulations [e.g., *Nagy et al.*, 2001; *Ma et al.*, 2006; *Sillanpää et al.*, 2006; *Modolo and Chanteur*, 2008]. These properties of ion transport in Titan's upper atmosphere are, at least qualitatively, analogous to those of Venus. Various works have shown that the ion distribution in the upper atmosphere of Venus presents appreciable departure from diffusive equilibrium. Such a departure has been interpreted as either a signature of ion escape [*Ghosh and Mahajan*, 1995] or responsible for the day-to-night ion flow [*Fox*, 2008].

[6] The purpose of this study is to investigate the general characteristics of ion transport in Titan's upper atmosphere through an analysis of the observed electron (or total ion) density profiles. We will address both ion escape and day-to-night ion flow. The structure of the article is as follows. In section 2, we describe the combined Cassini data set used for the study, and we also present the altitude profiles of various input parameters used for solving the momentum equation in later sections. We compare in section 3 the observed electron profiles with those in diffusive equilibrium, with the apparent departures used in section 4 to derive the ion flow velocities and fluxes. Finally we conclude in section 5.

2. Sample Description and Input Parameters

[7] This work is based on a multi-instrumental data set acquired during nine Titan flybys of the Cassini spacecraft, combining measurements made with INMS, RPWS, and the Cassini Magnetometer (MAG). The flybys included in this study are known in project parlance as T5, T17, T18, T21, T26, T32, T36, T39, and T40. Among these flybys, five (T17, T18, T36, T39, and T40) are at the dayside while the other four (T5, T21, T26, and T32) are at the nightside. The sample used for this study is similar to that included in our previous investigation of the diurnal variations of Titan's ionosphere [*Cui et al.*, 2009a].

[8] We show in Figure 1 various physical parameters as a function of altitude derived from the RPWS, INMS, and MAG measurements averaged over all flybys in our sample. These parameters include the electron (or total ion) density (from RPWS), electron temperature (from RPWS), mean ion mass (from INMS), and magnetic field strength (from MAG). The solid lines in Figure 1 give the empirical fits to the data (see section 3 for details). The strengths of both the total magnetic field, $|\mathbf{B}|$, and its horizontal component, $|B_h|$, are shown in Figure 1. Values of B_h are obtained with proper transform from the Kronographic (KRTP) coordinates to the

Titan Interaction System (TIIS) coordinates [e.g., *Neubauer et al.*, 2006]. Not too far from Titan, the TIIS components (B_r, B_θ, and B_ϕ) are close to KRTP (B_x, B_y, and B_z) except for the signs $B_r \approx -B_y$, $B_\theta \approx -B_z$, and $B_\phi \approx B_x$. Here B_r, B_θ, and B_ϕ are the radial, meridional, and azimuthal components of the magnetic field in TIIS with $B_h^2 = B_\theta^2 + B_\phi^2$; B_x, B_y, and B_z are the **B** components in KRTP. Figure 1 shows that in the global average sense, the **B** field is mostly horizontal at low altitudes but shows significant vertical component above ~1450 km. The MAG data are used to evaluate the magnetic force on the ionospheric plasma of Titan (see sections 3 and 4).

[9] The mean ion mass, $\overline{M}$ in Figure 1 is defined as $\overline{M} = \sum_i m_i N_i / N_e$, where m_i and N_i are the mass and number density of ion species i, N_e is the electron number density. The altitude profile of mean ion mass is used in later sections to determine the gravitational force. The ion densities, N_i, are obtained from the INMS data and their values rely on the appropriate choice of the spacecraft potential. In *Cui et al.* [2009a], we have adopted a constant value of −0.5 V for deriving the INMS ion densities. In this study, several choices of the INMS spacecraft potential are tested, and the corresponding influence on the derived mean ion mass is discussed in detail in Appendix A. It is worth emphasizing that the results presented in this paper rely on the INMS measurements through the parameter of mean ion mass, while the total ion density is taken from the RPWS data with the assumption of quasi-neutrality in Titan's ionosphere. Although the INMS ion densities could be quite sensitive to the choice of the spacecraft potential, the values of mean ion mass, which depend on ion density ratios, remain relatively stable.

[10] An intrinsic assumption in the derivation of ion densities from the INMS data is the neglect of ion wind in Titan's upper atmosphere. The effect of ion wind depends critically on the wind direction with respect to the INMS aperture normal, usually orientated along the direction of the spacecraft velocity. Ion wind along the aperture normal causes a decrease in ion sensitivity as a result of quad lens mistuning, while ion wind orthogonal to the aperture normal causes a decrease in sensitivity due to the deviation of the incident ion flow out of the center of the instrument field of view [*Waite et al.*, 2004; *Cravens et al.*, 2006]. Both effects are mass dependent, and the latter is usually more important than the former as a result of the small angular acceptance of the INMS when operating in the ion mode. For example, an orthogonal wind speed of ~0.3 km s^{-1} causes a decrease in sensitivity of light species such as CH_5^+ by ~25%, and a decrease in that of heavy species such as $C_6H_5^+$ by a factor of ~2. The influence of ion wind on our results is discussed in section 4.2.

3. Ion Distribution in Diffusive Equilibrium

[11] In diffusive equilibrium, the vertical component of the plasma momentum equation is given by

$$\frac{1}{N_e}\frac{\partial N_e}{\partial r} + \frac{1}{T_p}\frac{\partial T_p}{\partial r} + \frac{1}{H_p} + \frac{1}{N_e k T_p}\frac{\partial}{\partial r}\left(\frac{B_h^2}{8\pi}\right) = \sum_n \frac{\overline{M}\nu_n U_n}{kT_p}, \quad (1)$$

where $T_p = T_e + T_i$ is the plasma temperature with T_e and T_i being the electron and ion temperatures, N_e is the electron density, $\overline{M}$ is the mean ion mass defined in section 2, $H_p = (kT_p)/(\overline{M}g)$ is the plasma scale height with g being the local gravity and k being the Boltzmann constant, B_h is the magnitude of the horizontal **B** field, ν_n is the mean ion-neutral collision frequency, and U_n is the neutral drift velocity. The ion velocity, U_i, is ignored in equation (1) since we assume diffusive equilibrium. The derivation of equation (1) (and also equation (2) below) is provided in Appendix B.

[12] In equation (1), the first and second terms on the left-hand side give the plasma pressure gradient. The third and fourth terms are associated with gravitational and magnetic forces, respectively. The right-hand side term (summed over CH_4 and H_2) represents the effect of neutral drag, with ν_n estimated from the kinetic theory (see Appendix B) and U_n taken from *Yelle et al.* [2008] and *Cui et al.* [2008]. The drift motion of the background N_2 gas is ignored [e.g., *Strobel*, 2008]. We also assume a common temperature for all ion species. Such an assumption has been widely accepted in the studies of planetary ionospheres, since the differences in temperature between various ion species are usually negligible [e.g., *Kim et al.*, 1990]. We further assume that T_i is equal to the neutral temperature, T_n, with the latter taken from the empirical model of *Müller-Wodarg et al.* [2008]. *Roboz and Nagy* [1994] have predicted an ion temperature of ~300 K as a result of exothermic reactions. Despite this, the results of this study are not sensitive to the choice of T_i, since equation (1) depends only on the sum of T_i and T_e, and in all practical cases T_e is significantly higher than T_i. The thermal diffusion term, which is proportional to $\partial T_i/\partial r$, is ignored here for simplicity, since the gradient in electron temperature (typically 1–3 K km^{-1} from the RPWS data) is much larger than the gradient in ion temperature (typically of order 0.01 K km^{-1} from the temperature profile of *Müller-Wodarg et al.* [2008]).

[13] The electron distribution in diffusive equilibrium is obtained by integrating equation (1) upward from the lower boundary of 1250 km, with various input parameters derived from the INMS, RPWS, and MAG measurements (see section 2). The lower boundary is chosen to lie above the region of photochemical equilibrium [e.g., *Ma et al.*, 2006], as well as to avoid the uncertainty in mean ion mass due to the presence of heavy ions with $M/Z > 100$ not detected by the INMS [e.g., *Waite et al.*, 2007; J.-E. Wahlund, et al., On the amount of heavy molecular ions in Titan's ionosphere, submitted to *Planetary and Space Science*, 2009]. The electron density at the lower boundary is directly taken from the RPWS data. The approach adopted here is similar to that of *Hartle and Grebowsky* [1993] for the analysis of the nightside ionosphere of Venus. It is worth emphasizing that equation (1) is based on the assumption that horizontal variations are negligible. In a more general circumstance, equation (1) would contain terms proportional to the horizontal gradient of the **B** field components (i.e., $(B_\theta/r)(\partial B_r/\partial\theta) + (B_\phi/r \sin\theta)(\partial B_r/\partial\phi)$, see equation (B9)). Our approach is justified because we average all physical quantities derived from measurements over different flybys and this should effectively cancel out the horizontal variations. This horizontal averaging has proven effective in the study of the neutral atmosphere [*Cui et al.*, 2009b] and we assume that it applies as well to the ionized atmosphere.

[14] First, we show in Figure 2 (left) the observed electron (or total ion) density profile averaged over all flybys in our sample, given by the solid circles. Such a global average

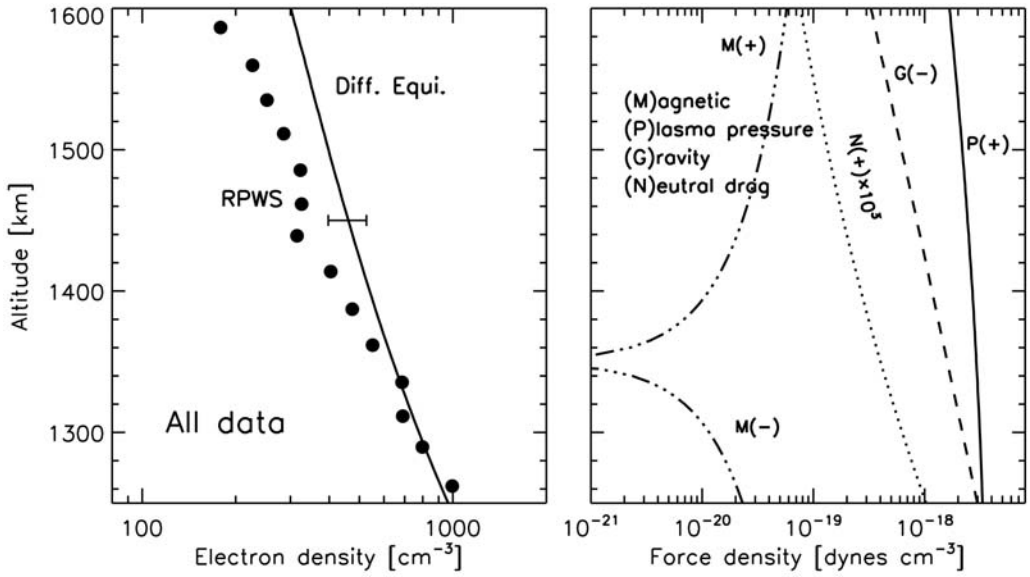

Figure 2. (left) Comparison between the observed RPWS electron density profile with that in diffusive equilibrium, in the global average sense. (right) The altitude profiles of various terms in the plasma momentum equation, including the plasma pressure gradient term, the gravitational term, the magnetic field term and the neutral drag term. The neutral drag term is amplified by a factor of 1000. Plus and minus signs represent upward and downward forces, respectively.

case will be revisited in section 4 to derive the total ion loss rate on Titan. Also shown in Figure 2 is the calculated profile assuming diffusive equilibrium, given by the solid line. The input parameters used for obtaining the diffusive equilibrium solution are adopted from the second-order log-polynomial fitting of the global average INMS, RPWS, and MAG data, as a function of altitude. These empirical fits are shown with the solid lines in Figure 1. Such a procedure helps avoiding kinks in the profiles of all parameters due to limited sampling but still preserves their prominent trends even though the fits are not perfect representations of the measurements (e.g., the fitting to the **B** field). The uncertainty in the diffusive equilibrium solution is also indicated in the figure at a reference altitude of 1450 km, estimated from a Monte Carlo approach taking into account uncertainties in the input parameters (see section 4.2 for details).

[15] Figure 2 shows that in the global average sense, the observed electron density profile is eroded above ~1400 km, compared to the diffusive equilibrium solution. This indicates that ion transport is important at high altitudes, consistent with the results of *Ma et al.* [2006] based on MHD model calculations (see their Figure 4). The electron distribution shown in Figure 2 is similar to that observed for the H^+ distribution in the nightside ionosphere of Venus [*Hartle and Grebowsky*, 1993]. The different electron density scale height, relative to diffusive equilibrium, is the signature of ion outflow, which carries ions away and reduces their densities. Since the electron distribution studied in this case is averaged over all flybys in our sample, we interpret the ion outflow as global ion escape from Titan.

[16] It is interesting to investigate in more detail how the ions are accelerated upward to escape from Titan. To do this, we present in Figure 2 (right) various terms of equation (1). These include the plasma pressure gradient term, the gravitational term, the magnetic field term, and the neutral drag term. The plus and minus signs represent upward and downward forces, respectively. The neutral drag term has been amplified by a factor of 10^3 in Figure 2, and it is clear that this term is significantly smaller than all the other terms. The magnetic force is directed downward below ~1350 km and upward above. However, since the magnetic force is small at all altitudes, the actual direction, which depends critically on the empirical fit, is not important here. The ion dynamics are primarily controlled by the upward plasma pressure gradient and the downward gravitational force. Near the lower boundary, the plasma pressure gradient and gravitational force are roughly in balance, leading to near diffusive equilibrium condition there. This is an impressive result since in this study diffusive equilibrium is directly obtained from the data rather than treated as a boundary condition. With increasing altitude, the plasma pressure gradient term increases more sharply than the gravitational term, producing a net force that drives upward ion acceleration and finally leads to ion escape from Titan. The net upward force density at the upper boundary is ~1.3×10^{-18} dynes cm^{-3}, corresponding to a net upward acceleration of ~210 cm s^{-2}. This is about a factor of 4 higher than the local gravity of ~51 cm s^{-2}.

[17] As mentioned in section 1, our previous analysis of an INMS sample similar to the one adopted here suggests that the primary source for the nightside ionosphere of Titan is the chemical survival of ions from the dayside [*Cui et al.*, 2009a]. This implies different patterns of ion transport at different local times on Titan. We investigate this possibility by considering two subsamples, one averaged over all dayside measurements with solar zenith angle, SZA < 90°

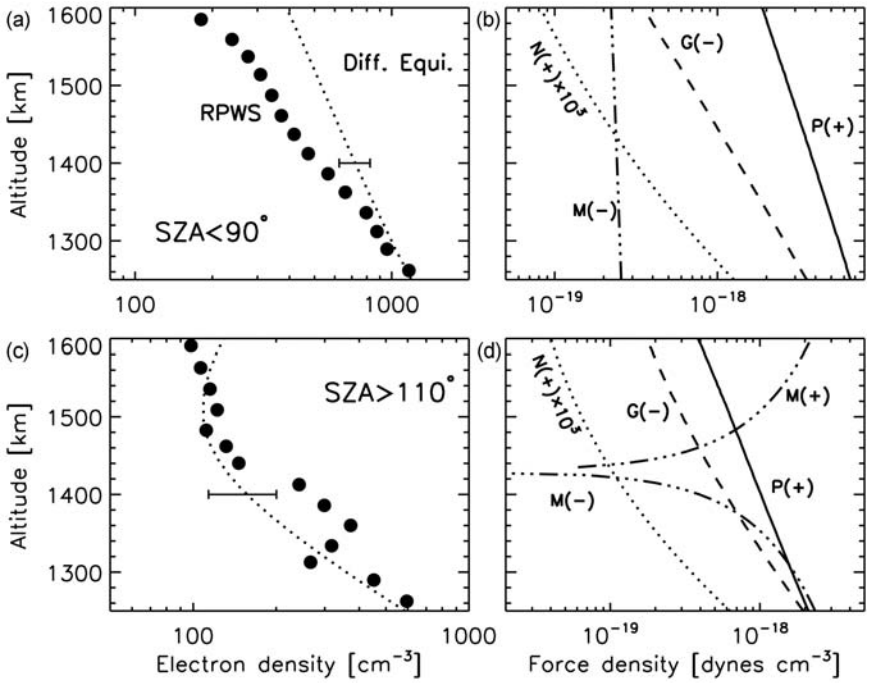

Figure 3. The same as Figure 2 but for the (a and c) dayside (with SZA < 90°) and (b and d) nightside (with SZA > 110°), respectively. Note that the two cases are not plotted with the same horizontal scale.

and the other one averaged over the nightside with SZA > 110°. The nightside subsample is defined to avoid significant photoionization near Titan's terminator [e.g., *Müller-Wodarg et al.*, 2000; *Ågren et al.*, 2009].

[18] We compare in Figures 3a and 3c the observed electron distributions with those in diffusive equilibrium, for the two cases. Typical uncertainties in the diffusive equilibrium profiles are indicated at a reference altitude of 1400 km. At the dayside (Figure 3a), the measured electron density profile is eroded as compared with the diffusive equilibrium solution, implying ion outflow, analogous to the global average case. However, such a dayside outflow may not imply net ion escape from Titan, since here the profile is averaged over some limited regions of the ionosphere (dayside) and the ions carried away by the outflow may simply return to some other regions (nightside). The same comparison for the nightside (Figure 3c) shows that the observed densities are enhanced over those in diffusive equilibrium. This suggests ion inflow at the nightside, analogous to the observation of O^+ distribution in the nightside ionosphere of Venus [*Hartle and Grebowsky*, 1993]. The different behaviors of ion transport between the dayside and nightside of Titan could be interpreted as a result of day-to-night ion transport, consistent with the scenario proposed in *Cui et al.* [2009a], though the two studies are based on completely different approaches. Also note that, strictly speaking, the presence of such horizontal ion flow implies nonnegligible horizontal velocity divergence term in the momentum equation, which we have ignored in equation (1). However, we do not expect that treating the momentum equation in a more strict way will lead to any significant change of our conclusions since the horizontal ion flow is one order of magnitude smaller than the vertical escaping flow (see section 4.3).

[19] The profiles of various force terms are shown in Figures 3b and 3d for both the dayside and nightside. Note that Figure 3b (dayside) and Figure 3d (nightside) are plotted with different horizontal scales. It can be seen from Figure 3 that the momentum budget at the dayside is similar to the global average case (i.e., primarily controlled by the plasma pressure gradient and gravity). However, the situation differs remarkably at the nightside. The magnetic field is important at nearly all altitudes (except for a narrow region near ~1430 km). This is due to the relatively low plasma pressure well beyond the terminator. Specifically, the day-to-night plasma pressure ratio ranges from ~3 at 1250 km to ~2 at 1600 km. Gravity also becomes more important at the nightside, as a result of the day-to-night difference in ion composition [*Cui et al.*, 2009a]. Below ~1420 km, the downward force (gravitational + magnetic) dominates over the upward plasma pressure gradient, leading to net downward ion acceleration at the nightside. However, at relatively high altitudes, ions are still accelerated upward, primarily driven by magnetic field rather than plasma pressure gradient.

[20] An alternative approach is to adopt the electron distribution from the RPWS data while treating the plasma temperature as the unknown to be solved from equation (1). This gives an estimate of the plasma temperature profile required by diffusive equilibrium, as shown by the solid lines in Figure 4a for the global average case, in Figure 4b for the dayside, and Figure 4c for the nightside. The solid circles in Figure 4 give the measured plasma temperatures, which is the sum of the RPWS electron temperatures and the INMS ion (neutral) temperatures. Figure 4 clearly shows that the ionospheric plasma in Titan's upper atmosphere is not in diffusive equilibrium condition. The temperature departure easily exceeds 1000 K, and such a large difference

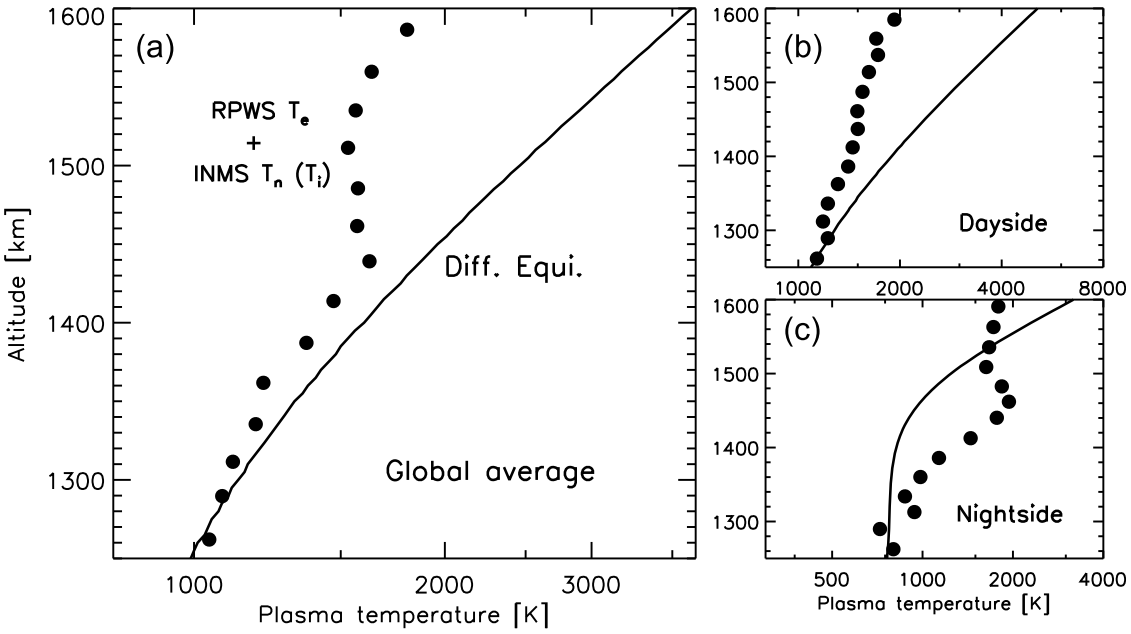

Figure 4. Comparison between the observed plasma temperature profile (solid circles) with that derived by assuming electron distribution in diffusive equilibrium (solid lines), for (a) the global average case, (b) the dayside, and (c) the nightside. The observed plasma temperature is taken to be the sum of the RPWS electron temperature and the INMS ion temperature. The latter is assumed to be identical to the neutral temperature given by the empirical model of *Müller-Wodarg et al.* [2008].

cannot be due to our approximate treatment of $T_i = T_n$ for the ion temperature [e.g., *Roboz and Nagy*, 1994].

[21] Finally, we note that the properties of ion transport may also vary with the magnetic field configuration in the vicinity of Titan, since ions preferentially escape along the magnetotail structures with open **B** field lines [e.g., *Nagy et al.*, 2001; *Sillanpää et al.*, 2006]. However, we find that both the total **B** field and its horizontal component are nearly identical for the dayside and nightside subsamples. This implies that open **B** field lines are not necessary for ion outflow on Titan at the altitudes under consideration.

4. Ion Transport in Titan's Upper Atmosphere

4.1. Extraction of Ion Velocity Profiles

[22] From the analysis above, we see that in general, the observed electron (or total ion) distribution in Titan's upper atmosphere cannot be described by the diffusive equilibrium model. We derive in this section the altitude profiles of ion drift velocity from the combined Cassini data set.

[23] In steady state, the vertical component of the plasma momentum equation is given by

$$\frac{\overline{M}U_i}{kT_p}\frac{\partial U_i}{\partial r}+\frac{1}{N_e}\frac{\partial N_e}{\partial r}+\frac{1}{T_p}\frac{\partial T_p}{\partial r}+\frac{1}{H_p}+\frac{1}{N_e kT_p}\frac{\partial}{\partial r}\left(\frac{B_h^2}{8\pi}\right) = -\frac{\overline{M}U_i}{kT_p}\nu, \tag{2}$$

where U_i is the ion drift velocity assumed to be common to all species, ν is the total ion-neutral collision frequency summed over N_2, CH_4, and H_2, and all other quantities have been defined above. The nonzero neutral drift velocities (for CH_4 and H_2) have been ignored here since the neutral drag due to these velocities is negligible (see Figures 3c and 3d and Figures 4b and 4c).

[24] At relatively low altitudes where the ion flow is expected to be subsonic, we can safely ignore the nonlinear term on the left-hand side of equation (2). In that case, it is straightforward to solve equation (2) for the ion drift velocity. On the other hand, with increasing altitude, the diffusion approximation may no longer be valid, and in this case we adopt the approach of *Hartle and Grebowsky* [1993] as outlined below.

[25] We combine equation (2) with the continuity equation,

$$\frac{1}{r^2}\frac{\partial}{\partial r}\left(r^2 N_e U_i\right) = P - L, \tag{3}$$

to remove the velocity derivative, $\partial U_i/\partial r$, where P and L are the electron (or total ion) production and loss rates. This gives the following nonlinear algebraic equation for ion velocity

$$\left(\frac{1}{N_e}\frac{\partial N_e}{\partial r}+\frac{2}{r}\right)U_i^2-\nu U_i = \frac{kT_p}{\overline{M}N_e}\frac{\partial N_e}{\partial r}+\frac{k}{\overline{M}}\frac{\partial T_p}{\partial r} + g+\frac{1}{\overline{M}N_e}\frac{\partial}{\partial r}\left(\frac{B_h^2}{8\pi}\right), \tag{4}$$

where the production and loss terms have been ignored since in the altitude range considered here, the ion-neutral collision rate is significantly higher than the ion production and loss rates (see Appendix B). Except for ion velocity, all other quantities (as well as their derivatives) in equation (4) can be directly obtained from the INMS, RPWS, and MAG data. Equation (4) can be solved straightfowardly, which does not require any boundary condition to be specified. Also note

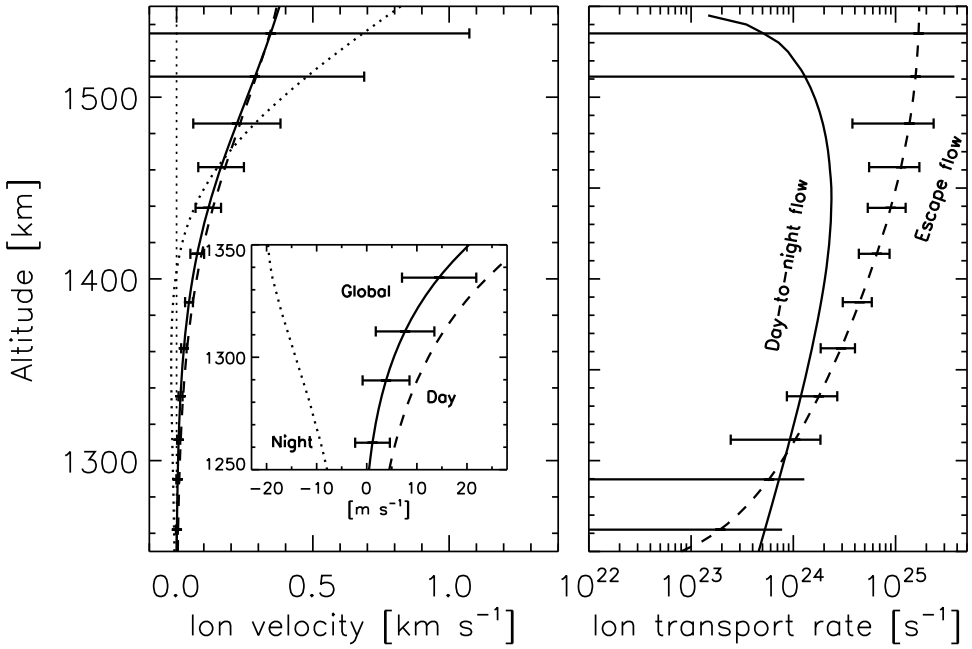

Figure 5. (left) The altitude profiles of ion drift velocity derived from the vertical component of the plasma momentum equation, for the global average case (solid line), the dayside (dashed line), and the nightside (dotted line). Also shown are the 1 σ uncertainties in global average ion velocity estimated with a Monte Carlo approach (see section 4.2). The insert enlarges the day-to-night difference in ion velocity below 1350 km. (right) The horizontal transport rate (solid line) and vertical transport rate (dashed line, with 1σ uncertainties), as a function of altitude. The former is associated with day-to-night ion flow while the latter characterizes global ion escape from Titan.

that, generally speaking, equation (4) gives two sets of solution, of which the correct one can be selected based on a transition in the property of the equation from low to high altitudes (see *Hartle and Grebowsky*, 1993 for details). We find that the solutions to equation (2) (ignoring the nonlinear term on the left-hand side, valid at low altitudes) and to equation (4) are very close from the lower boundary (1250 km) up to 1400 km.

[26] The derived ion velocity profiles are presented in the Figure 5 (left), with 1σ uncertainties (see section 4.2 for details). The global average ion velocity (given by the solid line) starts from very small values near the lower boundary and increases to ~0.5 km s^{-1} near 1600 km. The ion-acoustic velocity, $U_s = \sqrt{kT_p/\overline{M}}$, ranges from ~0.5 km s^{-1} at 1250 km to ~0.8 km s^{-1} at 1600 km as a result of increasing plasma temperature and decreasing mean ion mass with increasing altitude. Accordingly, the ion outflow remains subsonic throughout the altitude region considered here. The derived ion velocities are significantly larger than the drift velocities of neutral species such as CH_4 and H_2, of which the former does not exceed 0.01 km s^{-1} [*Yelle et al.*, 2008] and the latter does not exceed 0.1 km s^{-1} [*Cui et al.*, 2008] in the same altitude region.

[27] The dashed and dotted lines in Figure 5 (left) give the ion velocity profiles for the dayside and nightside, respectively. The dayside velocity profile is close to the global average case, since the global average electron densities are dominated by dayside values [e.g., *Ågren et al.*, 2009]. Diurnal velocity difference is clearly seen, especially below ~1400 km where the dayside velocities are upward and the nightside velocities are downward (see Figure 5, insert). The velocity difference is more than 3σ for this altitude range. Such a diurnal difference is consistent with what expected from Figure 3 and implies the presence of day-to-night ion flow in Titan's upper atmosphere. Above ~1400 km, both cases show upward ion velocities. The confidence level of velocity difference decreases with increasing altitude and is within 1σ above ~1450 km. Such a feature could be interpreted by the fact that ion transport at high altitudes is dominated by ion escape at both the dayside and nightside, and such an ion escape does not present strong diurnal variation. As a consequence, the observed day-to-night difference in ion velocity is interpreted in this article as a combined result of global ion escape and day-to-night ion transport. A more quantitative assessment of this scenario is provided in section 4.3.

4.2. Uncertainties in Ion Velocities

[28] As mentioned in section 2, one uncertainty in the determination of the INMS ion densities is the neglect of ion wind. Below ~1450 km, the derived ion velocities are generally smaller than 0.2 km s^{-1}, as shown in Figure 5 (left). As a consequence, the decrease in ion sensitivity due to ion wind is insignificant and it is a good approximation to derive the INMS ion densities assuming a stationary ionosphere. At higher altitudes, the ion wind could be fast enough that the change in ion sensitivity becomes large, especially when the wind direction is orthogonal to the INMS aperture normal. This indicates that the velocity profiles below ~1450 km are more reliable than those above. However, it is worth mentioning that the electron (or total

ion) densities adopted for extracting the velocity profiles are directly taken from the RPWS measurements, which are typically known within 10% and for which the uncertainties discussed above are not a concern. In fact, the influence of ion wind on the derived velocity profiles is associated with the determination of mean ion mass and to a lesser extent, mean ion-neutral collision frequency (see Appendix B). These are the only two input parameters in our calculations that rely on the INMS ion measurements.

[29] The effect of ion wind on the determination of mean ion mass is difficult to estimate quantitatively, since it relies critically on the wind orientation with respect to the INMS aperture normal. When averaged over several flybys, such an effect does not necessarily cancel out since it always causes a decrease in ion sensitivity (see section 2). For the same wind speed, the decrease in the sensitivity of heavy ions is larger than that of light ions, implying underestimated mean ion mass. However, since the effect of ion wind on sensitivity is important only at high altitudes where the densities of heavy ions tend to be small [e.g., *Cui et al.*, 2009a], we expect that the uncertainties in mean ion mass associated with ion wind may not be very large.

[30] We test the sensitivity of the derived ion velocities to input parameters with a Monte Carlo approach. The values of several input parameters (T_e, N_e, $|B_h|$) are assumed to satisfy the Gaussian distribution, with the mean taken from the data and the standard deviation taken to be at a 1%–30% level. More specifically, we assign a 5% level uncertainty to RPWS electron density and temperature. This is smaller than the typical uncertainty of 10% in individual RPWS measurements, since the input parameters are averaged over several flybys. The uncertainty in the **B**-field strength, which arises from the very slight nonorthogonality of the triaxial sensors in the Fluxgate Magnetometer (FGM) and interference from the spacecraft field, is typically very small and assigned to be 1% [*Dougherty et al.*, 2004]. However, for the mean ion mass and ion-neutral collision frequency, we assume an uncertainty of 30% to account for the potential large errors in these parameters. For each random realization of the input parameters, we solve equation (4) for the ion velocity profile according to the procedure outlined in section 4.1. We investigate the distribution of the extracted ion velocities at different altitudes, based on a total number of 10^4 random realizations.

[31] The uncertainties in the global average ion velocity, estimated from the Monte Carlo approach outlined above, are given in Figure 5 (left) at different altitudes. We find that ion velocities are relatively well constrained below ~1450 km but less constrained above. This is related to our procedure of adopting the empirical fits to the input parameters for solving the momentum equation, because although the values of each parameter may fluctuate considerably between different random samples, the empirical fit, which characterizes the overall trend, remains relatively stable.

[32] Finally, we emphasize that the ion velocity profiles presented in this study are based on the Cassini data acquired during nine close Titan flybys, including five at the dayside and four at the nightside. Combining a large data set is to remove as much as possible the horizontal variations so that the vertical momentum equations (equations (3) and (4)) are valid. As a test of the validity of such an assumption and also as an assessment of the variance due to limited sampling, we adopt a simple bootstrapping technique in which we solve equation (4) for the ion velocity profile by excluding one single flyby from our complete sample. This is repeated for all flybys, and we investigate the difference in ion velocity between the resulting nine subsamples, each of which contains the data from eight different Titan flybys. We find that the uncertainty in ion velocity estimated from the procedure outlined above increases from less than 10 m s^{-1} below ~1350 km to ~150 m s^{-1} at 1600 km. This indicates that the main conclusions made in this article are not sensitive to any single data set, though considerable variations are present between different flybys [e.g., *Ågren et al.*, 2009].

4.3. Ion Fluxes

[33] The ion velocity profile, as shown in Figure 5 (left), when multiplied by the electron (or total ion) density, gives the ion flux. In order to determine the total ion loss rate on Titan, we need to estimate the location of the ion exobase. This is derived from the condition of $H_e = \lambda$, where H_e is the observed scale height of electron distribution (to be distinguished from the plasma scale height, H_p given in equations (1) and (2)) and $\lambda = U_{\rm th}/\nu$ is the ion mean free path with $U_{\rm th} = \sqrt{(8kT_i)/(\pi\overline{M})}$ being the ion thermal velocity (to be distinguished from the ion-acoustic velocity, U_s defined in section 4.1) and ν being the total ion-neutral collision frequency given in equation (2). H_e is estimated to be ~190 km from the slope of the global average RPWS electron distribution (between 1400 and 1700 km). Inserting appropriate values for the other parameters gives the location of Titan's ion exobase at ~1550 km, which is slightly higher than the neutral exobase height of ~1450–1500 km [e.g., *Cui et al.*, 2008]. Taking the global average ion flux of ~$(8 \pm 2) \times 10^6$ cm^{-2} s^{-1} and the mean ion mass of ~24.5 amu at the ion exobase (see Figure 1), we find a total ion loss rate of ~$(1.7 \pm 0.4) \times 10^{25}$ s^{-1} or ~700 ± 170 g s^{-1} on Titan. The latter value might be underestimated due to the decrease in ion sensitivity associated with ion wind (see section 4.2).

[34] The ion loss rate given above is ~70% higher than the value of ~10^{25} s^{-1} estimated by *Wahlund et al.* [2005] based on the RPWS data acquired during the TA and TB flybys. Our value lies between the ion loss rate of ~$(3–7) \times 10^{24}$ s^{-1} predicted by MHD models [e.g., *Nagy et al.*, 2001; *Ma et al.*, 2006] and the value of ~$(1.5–6) \times 10^{25}$ s^{-1} predicted by hybrid simulations [e.g., *Sillanpää et al.*, 2006; *Modolo and Chanteur*, 2008]. The total ion mass loss rate that we derive is significantly higher than the value of ~50–104 g s^{-1} given by *Ma et al.* [2006]. This does not seem to be due to the neglect of relatively heavy ions, since *Ma et al.* [2006] did include ions up to $M/Z \sim 74$ in their MHD model. An assessment of such a discrepancy requires a careful comparison of the loss rates of individual ion species, which will be attempted in a follow-up study. Finally, we note that the ion loss rate is significantly smaller than the neutral loss rate of ~1.1×10^{28} s^{-1} or ~7.6×10^4 g s^{-1} [*Strobel*, 2009].

[35] The ion flux derived for the dayside and nightside of Titan should be interpreted with some caution, and day-to-night ion flow needs to be taken into account. We assume that the ion loss rates are about equal for both sides since no significant diurnal variation is observed for the ion flow velocity above ~1450 km (see section 4.2). At any given

altitude, the total number of ions removed from the dayside per unit time is $\sim 2\pi r^2 F_{day}$, of which $\sim 2\pi r^2 F_{global}$ escape and accordingly $\sim 2\pi r^2 (F_{day} - F_{global})$ go horizontally to the nightside. Here F_{day} and F_{global} stand for the dayside ion flux and global average ion flux. A similar expression can be obtained for the nightside, and taking the average of the two gives an estimate of the horizontal ion transport rate of $\sim \pi r^2 (F_{day} - F_{night})$, where F_{night} is the nightside ion flux. The horizontal ion transport rate is presented in Figure 5 (right) as a function of altitude. Also shown in Figure 5 is the vertical transport rate associated with ion escape (with 1 σ error bars), estimated from $4\pi r^2 F_{global}$. The horizontal ion transport rate is not strongly dependent on altitude below the ion exobase, with an average value of $\sim (1.4 \pm 0.5) \times 10^{24}$ s^{-1} or, equivalently, a mass transport rate of $\sim (45 \pm 15)$ g s^{-1}. The former value is consistent with the corotational ion flow of $\sim (1.2–1.4) \times 10^{24}$ s^{-1} estimated by *Sillanpää et al.* [2006] based on hybrid simulation. However, their mass transport rate of ~19–23 g s^{-1} is about a factor of 2 lower, probably because ions heavier than 28 amu were not taken into account in that work. Figure 5 shows that although significant day-to-night ion flow is present at least up to ~1550 km, the vertical ion outflow is still dominant, except below ~1300 km.

[36] Finally, it is interesting to compare the day-to-night horizontal ion flow with the total ion loss rate integrated over Titan's nightside. For a rough estimate, we consider electron recombination only and ignore ion loss by ion-neutral reactions. The latter is important only for light and short-lived ion species, which have a modest contribution to the nightside ionosphere of Titan compared with heavy and long-lived ions [*Cui et al.*, 2009b]. To estimate the total recombination rate, we adopt the typical recombination coefficient of $\sim 7 \times 10^{-7}$ cm^3 s^{-1} [*Vuitton et al.*, 2007], a typical nightside electron density of ~200 cm^{-3} (see Figure 1). This gives the total recombination rate of $\sim 2 \times 10^{24}$ s^{-1} integrated over the nightside hemisphere and over the altitude range considered here. The integrated total recombination rate is comparable with the day-to-night horizontal ion flow inferred above, indicating that transport is an important source for Titan's nightside ionosphere.

5. Concluding Remarks

[37] We present an in-depth study of the properties of ion transport in Titan's upper atmosphere between 1250 and 1600 km, based on a combined Cassini data set, including INMS, RPWS, and MAG data acquired during nine Cassini flybys with the satellite. We adopt the electron temperature and electron (or total ion) density from RPWS, mean ion mass from INMS, and **B**-field strength from MAG.

[38] We investigate the electron distribution in the global average sense, as well as for the dayside and nightside of Titan. The observed electron density profiles depart from diffusive equilibrium, implying significant ion transport in Titan's upper atmosphere. The departures from diffusive equilibrium are used to derive the ion velocity profiles in this article.

[39] We summarize the main results of this article as follows. (1) There is clear evidence for global ion escape on Titan, with a total ion loss rate of $\sim (1.7 \pm 0.4) \times 10^{25}$ s^{-1}, consistent with that estimated by *Wahlund et al.* [2005] based on the RPWS measurements. (2) Significant difference is present in the pattern of ion transport between the dayside and nightside of Titan, characterized by dayside ion outflow and nightside ion inflow, especially below ~1400 km. We interpret this as a result of day-to-night ion transport, with a horizontal transport rate of $\sim (1.4 \pm 0.5) \times 10^{24}$ s^{-1}. Such a flow contributes to the production of an appreciable ionosphere at Titan's nightside, consistent with the scenario proposed in *Cui et al.* [2009a].

Appendix A: Choice of the INMS Spacecraft Potential

[40] The determination of ion densities from the INMS data relies on the choice of the spacecraft potential, which influences the instrument sensitivity to ions by modifying their trajectories relative to the spacecraft [*Waite et al.*, 2004]. In *Cui et al.* [2009a], a constant value of −0.5 V was adopted for calculating the ion densities. An alternative choice is to use the spacecraft potentials derived from other instruments such as RPWS and CAPS (J.-E. Wahlund et al., submitted manuscript, 2009; F. J. Crary et al., Heavy and negative ions at Titan measured by Cassini CAPS, submitted to *Plan. Space Sci.*, 2009), which in general vary with altitude. However, the spacecraft potentials at different locations of Cassini may also differ, therefore adopting the potentials from other instruments does not necessarily give the correct results though in some cases these results are satisfactory [e.g., *Cui et al.*, 2009a; J.-E. Wahlund et al., submitted manuscript, 2009].

[41] In this work, we propose a new way of analyzing the INMS ion data in which the spacecraft potential is treated as a free parameter, to be determined by requiring that the corresponding INMS total ion densities are equal to the RPWS electron densities, for all measurements made above 1250 km. As mentioned in section 2, this lower boundary altitude is chosen to ensure that the contribution from heavy positive ions with $M/Z > 100$ can be safely ignored [e.g., *Waite et al.*, 2007; J.-E. Wahlund et al., submitted manuscript, 2009].

[42] An example is illustrated in Figure A1, for the inbound T17 flyby. Figure A1 (left) shows with the dashed lines the total ion density profiles calculated with several choices of constant INMS spacecraft potential of −2 V, −0.5 V, and 2 V. The RPWS electron density profile is given by the solid line. Setting the INMS total ion densities equal to the RPWS electron densities gives an estimate of the INMS spacecraft potential, as indicated by the solid line in Figure A1 (right). For comparison, we show the RPWS spacecraft potential by the dashed line. It is clear from Figure A1 that the abrupt transition in the INMS total ion density profile near ~1380 km, which is not observed in the RPWS electron profile, can be interpreted as a result of change in the INMS spacecraft potential at the same altitude. Such a change is also seen in the RPWS spacecraft potential, though to a lesser extent.

[43] Figure A1 shows that the variation of total ion density with spacecraft potential is not monotonic. This implies that at any given altitude, there are in general two values of spacecraft potential for which the INMS total ion densities are equal to the RPWS electron densities. In such cases, we always adopt the value of the INMS spacecraft potential that is closer to the RPWS spacecraft potential. In addition, due

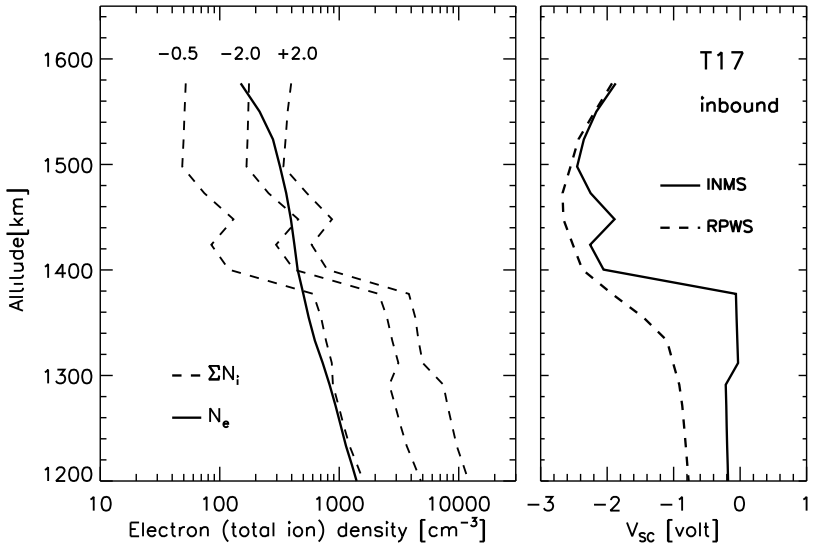

Figure A1. The INMS total ion and RPWS electron densities for the inbound T17 flyby. (Left) The dashed lines give the INMS total ion density profiles calculated with several choices of constant spacecraft potential: −2 V, −0.5 V, and 2 V. The solid line represents the RPWS electron density profile. (Right) The solid and dashed lines give the INMS and RPWS spacecraft potentials as a function of altitude.

to the nonmonotonic nature described above, there is a minimum possible value of total ion density at a given altitude. Occasionally, these minimum values are higher than the RPWS electron densities with residual difference typically within 10%. In such cases, we simply adopt the INMS spacecraft potentials that give the minimum values of total ion density. The INMS spacecraft potential is usually negative but sometimes becomes positive due to the emission of photoelectrons from the surface of the spacecraft. It is also worth mentioning that the estimated spacecraft potentials should be used with caution when they exceed +/−2 V, since the impacting ions are shifted to regions of the transmission curve with low efficiency [*Waite et al.*, 2004].

[44] Finally, we compare the mean ion mass for different choices of the INMS spacecraft potential, since this is the only parameter in this study that relies on the INMS ion data. We find that throughout the altitude region of our interest (between 1250 and 1600 km), the mean ion mass profiles are usually in agreement within 5% but could occasionally differ by ~10% (such as below ~1300 km for the T21 flyby). However, in all cases the uncertainty in mean ion mass due to the detailed choice of spacecraft potential is significantly smaller than that due to ion wind (see section 2). An assessment of the sensitivity of our results on ion wind is presented in section 4.2.

Appendix B: Plasma Momentum Equation in Titan's Ionosphere

[45] For application to planetary ionospheres, the momentum equation for either the single plasma fluid or individual ion species has been presented in various works. However, the form of the equation is not always consistent, and the inherent approximations have not been validated in a careful way. We present in this appendix a derivation of the plasma momentum equation adopted for this study.

[46] In steady state, the momentum equation for individual ion species is given by

$$N_i m_i \mathbf{U}_i \cdot \nabla \mathbf{U}_i + \nabla p_i - n_i e\left(\mathbf{E} + \frac{1}{c}\mathbf{U}_i \times \mathbf{B}\right) - N_i m_i \mathbf{G} = -N_i m_i \sum_n \nu_{in}(\mathbf{U}_i - \mathbf{U}_n) - m_i \mathbf{U}_i (P_i - L_i), \quad \text{(B1)}$$

where p_i, N_i, m_i are the pressure, number density, and mass of species i, e is the electron charge, **E** and **B** are the electric and magnetic fields, **G** is the local gravity, $\mathbf{U_n}$ and $\mathbf{U_i}$ are the neutral and ion drift velocities, ν_{in} is the ion-neutral collision frequency, and P_i and L_i are the ion production and loss rates. The momentum equation for thermal electrons can be expressed as

$$\nabla p_e + N_e e\left(\mathbf{E} + \frac{1}{c}\mathbf{U}_e \times \mathbf{B}\right) = 0, \quad \text{(B2)}$$

where p_e, N_e, and $\mathbf{U_e}$ are the electron pressure, density, and drift velocity and all other terms proportional to electron mass have been ignored. The electric field, **E**, can be removed by adding equation (B2) and the sum of equation (B1) over all ion species. This gives

$$\sum_i N_i m_i \mathbf{U}_i \cdot \nabla \mathbf{U}_i + \nabla\left(p_e + \sum_i p_i\right) - \frac{\mathbf{J} \times \mathbf{B}}{c} - \sum_i N_i m_i \mathbf{G} = -\sum_i \sum_n N_i m_i \nu_{in}(\mathbf{U}_i - \mathbf{U}_n) - \sum_i m_i \mathbf{U}_i (P_i - L_i), \quad \text{(B3)}$$

where $\mathbf{J} = -N_e e \mathbf{U}_e + \sum_i N_i e \mathbf{U}_i$ is the current density, and we have also assumed charge neutrality, i.e., $\sum_i N_i = N_e$.

[47] Recasting the current density in equation (B3) with the Ampère's law and the ion and electron pressures with the ideal gas law, we have

$$N_e\overline{M}\mathbf{U}_i\cdot\nabla\mathbf{U}_i + kT_p\nabla N_e + kN_e\nabla T_p - \frac{(\nabla\times\mathbf{B})\times\mathbf{B}}{4\pi} - N_e\overline{M}\mathbf{G} = -\sum_i\sum_n N_i m_i\nu_{in}(\mathbf{U}_i-\mathbf{U}_n), \quad \text{(B4)}$$

where k is the Boltzmann constant, $T_p = T_i + T_e$ is the plasma temperature with T_i and T_e being the ion and electron temperatures, and $\overline{M} = \sum_i N_i m_i/N_e$ is the mean ion mass and we have also assumed a common ion temperature, T_i, and common ion velocity, $\mathbf{U}_i$, for different species. An inherent assumption in applying the Ampère's law is a constant $\mathbf{B}$ field produced by the dynamo in Saturn's interior as well as the ring current in the magnetosphere, which means that the derivative of $\mathbf{B}$ field includes only the perturbation field from Saturn's magnetospheric interaction with Titan. The production and loss terms in equation (B3) have been ignored since they are significantly smaller than the collision term. This can be seen by comparing the total ion loss rate with the total ion-neutral collision rate. The former can be estimated from the total recombination rate, since the production and loss of individual ion species through ion-neutral reactions cancel out when summing over all species. From the measured RPWS electron densities, we estimate the total ion loss rate to be ~0.5 cm^{-3} s^{-1} at 1250 km and ~7 × 10^{-3} cm^{-3} s^{-1} at 1600 km, where we adopt the recombination coefficients from *Vuitton et al.* [2007] for different ion species. These values are significantly smaller than the total ion-neutral collision rate of ~0.2–200 cm^{-3} s^{-1} for the same altitude range (see below for a discussion of the appropriate collision frequency to be used).

[48] Following *Schunk and Nagy* [2000], the ion-neutral collision frequency is evaluated from the kinetic theory,

$$\nu_{in} = 2.21\pi\frac{N_n m_n}{m_i+m_n}\sqrt{\frac{\gamma_n e^2}{\mu_{in}}}, \quad \text{(B5)}$$

where γ_n is the neutral polarizability and $\mu_{in} = m_i m_n/(m_i + m_n)$ is the reduced mass with m_n being the neutral mass. After some algebra, the right-hand side of equation (B4) can be recast as

$$\sum_i\sum_n N_i m_i\nu_{in}(\mathbf{U}_i-\mathbf{U}_n) = N_e\overline{M}\sum_n\nu_n(\mathbf{U}_i-\mathbf{U}_n), \quad \text{(B6)}$$

where ν_n is the mean ion-neutral collision frequency (for neutral species n) defined as

$$\nu_n = 2.21\pi\frac{N_n m_n}{\overline{M}+m_n}\sqrt{\frac{\gamma_n e^2}{\mu_n}}\sum_i\frac{N_i}{N_e}\sqrt{\frac{m_i(\overline{M}+m_n)}{\overline{M}(m_i+m_n)}}, \quad \text{(B7)}$$

with $\mu_n = \overline{M}m_n/(\overline{M} + m_n)$. Note that equation (B7) is not an analog of equation (B5) with the individual ion mass m_i replaced with the mean ion mass $\overline{M}$, due to the presence of an additional dimensionless factor (with a value of ~1–1.2 for the altitude range considered in this study).

[49] Combining equations (B4) and (B6), we have

$$N_e\overline{M}\mathbf{U}_i\cdot\nabla\mathbf{U}_i + kT_p\nabla N_e + kN_e\nabla T_p + \nabla\left(\frac{B^2}{8\pi}\right) - \frac{(\mathbf{B}\cdot\nabla)\mathbf{B}}{4\pi} - N_e\overline{M}\mathbf{G} = -N_e\overline{M}\sum_n\nu_n(\mathbf{U}_i-\mathbf{U}_n), \quad \text{(B8)}$$

where we have used the appropriate vector relation to recast the magnetic field term. The radial component of the above equation is

$$N_e\overline{M}U_i\frac{\partial U_i}{\partial r} + kT_p\frac{\partial N_e}{\partial r} + kN_e\frac{\partial T_p}{\partial r} + N_e\overline{M}g + \frac{\partial}{\partial r}\left(\frac{B^2-B_r^2}{8\pi}\right) - \frac{1}{4\pi}\left(\frac{B_\theta}{r}\frac{\partial B_r}{\partial\theta} + \frac{B_\phi}{r\sin\theta}\frac{\partial B_r}{\partial\phi}\right) = -N_e\overline{M}\sum_n\nu_n(U_i-U_n), \quad \text{(B9)}$$

[50] which is used in sections 3 and 4 for deriving the properties of ion transport in Titan's upper atmosphere.

[51] **Acknowledgments.** J.C. and M.G. are supported by the Science and Technology Facilities Council (STFC) rolling grant to Imperial College London. R.V.Y. acknowledges support from NASA through grant NAG5-12699 to the University of Arizona and subcontract 699083KC from the Southwest Research Institute. J.H.W. is funded by NASA and the Jet Propulsion Laboratory contract 1283095 with the Southwest Research Institute. We acknowledge K. E. Mandt for discussions on the INMS ion data analysis and N. Achilleos for useful help with the MAG coordinate transform.

[52] Wolfgang Baumjohann thanks Darrell Strobel and the other reviewers for their assistance in evaluating this manuscript.

References

Ågren, K., et al. (2007), On magnetospheric electron impact ionization and dynamics in Titan's ram-side and polar ionosphere - a Cassini case study, *Ann. Geophys.*, *25*, 2359–2369.

Ågren, K., J.-E. Wahlund, P. Garnier, R. Modolo, J. Cui, M. Galand, and I. C. F. Müller-Wodarg (2009), The ionospheric structure of Titan, *Plan. Space Sci.*, in press.

Ajello, J. M., M. H. Stevens, I. Stewart, K. Larsen, L. Esposito, J. Colwell, W. McClintock, G. Holsclaw, J. Gustin, and W. Pryor (2007), Titan airglow spectra from cassini ultraviolet imaging spectrograph (UVIS): EUV analysis, *Geophys. Res. Lett.*, *34*, L24204, doi:10.1029/2007GL031555.

Bird, M. K., R. Dutta-Roy, S. W. Asmar, and T. A. Rebold (1997), Detection of Titan's Ionosphere from Voyager 1 Radio Occultation Observations, *Icarus*, *130*, 426–436, doi:10.1006/icar.1997.5831.

Brannon, J. F., J. L. Fox, and H. S. Porter (1993), Evidence for day-to-night ion transport at low solar activity in the Venus pre-dawn ionosphere, *Geophys. Res. Lett.*, *20*, 2739–2742, doi:10.1029/93GL02422.

Cravens, T. E., S. L. Crawford, A. F. Nagy, and T. I. Gombosi (1983), A two-dimensional model of the ionosphere of Venus, *J. Geophys. Res.*, *88*, 5595–5606, doi:10.1029/JA088iA07p05595.

Cravens, T. E., et al. (2005), Titan's ionosphere: Model comparisons with Cassini Ta data, *Geophys. Res. Lett.*, *32*, L12108, doi:10.1029/2005GL023249.

Cravens, T. E., et al. (2006), Composition of Titan's ionosphere, *Geophys. Res. Lett.*, *33*, L07105, doi:10.1029/2005GL025575.

Cravens, T. E., et al. (2008), Model-data comparisons for Titan(tm)s nightside ionosphere, *Icarus*, *199*, 174–188, doi:10.1016/j.icarus.2008.09.005.

Cui, J., R. V. Yelle, and K. Volk (2008), Distribution and escape of molecular hydrogen in Titan's thermosphere and exosphere, *J. Geophys. Res.*, *113*, E10004, doi:10.1029/2007JE003032.

Cui, J., M. Galand, R. V. Yelle, V. Vuitton, J.-E. Wahlund, P. P. Lavvas, I. C. F. Müller-Wodarg, T. E. Cravens, W. T. Kasprzak, and J. H. Waite Jr. (2009a), Diurnal variations of Titan's ionosphere, *J. Geophys. Res.*, *114*, A06310, doi:10.1029/2009JA014228.

Cui, J., et al. (2009b) Analysis of Titan's neutral upper atmosphere from Cassini Ion Neutral Mass Spectrometer measurements, *Icarus*, *200*, 581–615, doi:10.1016/j.icarus.2008.12.005.

Dougherty, M. K., et al. (2004) The Cassini Magnetic Field Investigation, *Space Sci. Rev.*, *114*, 331–383, doi:10.1007/s11214-004-1432-2.

Fox, J. L. (2008) Morphology of the dayside ionosphere of Venus: Implications for ion outflows, *J. Geophys. Res.*, *113*, E11001, doi:10.1029/2008JE003182.

Galand, M., J. Lilensten, D. Toublanc, and S. Maurice (1999), The ionosphere of titan: Ideal diurnal and nocturnal cases, *Icarus*, *140*, 92–105, doi:10.1006/icar.1999.6113.

Galand, M., R. V. Yelle, A. J. Coates, H. Backes, and J.-E. Wahlund (2006), Electron temperature of Titan's sunlit ionosphere, *Geophys. Res. Lett.*, *33*, L21101, doi:10.1029/2006GL027488.

Gan, L., C. N. Keller, and T. E. Cravens (1992), Electrons in the ionosphere of Titan, *J. Geophys. Res.*, *97*(A8), 12137–12151, doi:10.1029/92JA00300.

Ghosh, S., and K. K. Mahajan (1995), Evidence of upward H^+ flow in the Venus dayside ionosphere, *J. Geophys. Res.*, *100*(A11), 21,317–21,322, doi:10.1029/95JA01933.

Hartle, R. E., and J. M. Grebowsky (1993), Light ion flow in the nightside ionosphere of Venus, *J. Geophys. Res.*, *98*(E4), 7437–7445, doi:10.1029/93JE00399.

Ip, W.-H. (1990) Titan's upper ionosphere, *Astrophys. J.*, *362*, 354–363, doi:10.1086/169271.

Keller, C. N., T. E. Cravens, and L. Gan (1992), A model of the ionosphere of Titan, *J. Geophys. Res.*, *97*(A8), 12,117–12,135, doi:10.1029/92JA00231.

Kim, J., A. F. Nagy, T. E. Cravens, and H. Shinagawa (1990), Temperatures of individual ion species and heating due to charge exchange in the ionosphere of Venus, *J. Geophys. Res.*, *95*(A5), 6569–6573, doi:10.1029/JA095iA05p06569.

Kliore, A. J., et al. (2008), First results from the Cassini radio occultations of the Titan ionosphere, *J. Geophys. Res.*, *113*, A09317, doi:10.1029/2007JA012965.

Ma, Y.-J., A. F. Nagy, I. V. Sokolov, and K. C. Hansen (2004), Three-dimensional, multispecies, high spatial resolution MHD studies of the solar wind interaction with Mars, *J. Geophys. Res.*, *109*, A07211, doi:10.1029/2003JA010367.

Ma, Y.-J., A. F. Nagy, T. E. Cravens, I. V. Sokolov, K. C. Hansen, J.-E. Wahlund, F. J. Crary, A. J. Coates, and M. K. Dougherty (2006), Comparisons between MHD model calculations and observations of Cassini flybys of Titan, *J. Geophys. Res.*, *111*, A05207, doi:10.1029/2005JA011481.

Modolo, R., and G. M. Chanteur (2008), A global hybrid model for Titan's interaction with the Kronian plasma: Application to the Cassini Ta flyby, *J. Geophys. Res.*, *113*, A01317, doi:10.1029/2007JA012453.

Müller-Wodarg, I. C. F., R. V. Yelle, M. Mendillo, L. A. Young, and A. D. Aylward (2000), The thermosphere of Titan simulated by a global three-dimensional time-dependent model, *J. Geophys. Res.*, *105*, 20833–20856, doi:10.1029/2000JA000053.

Müller-Wodarg, I. C. F., R. V. Yelle, J. Cui, and J. H. Waite Jr. (2008), Horizontal structures and dynamics of Titan's thermosphere, *J. Geophys. Res.*, *113*, E10005, doi:10.1029/2007JE003033.

Nagy, A. F., Y. Liu, K. C. Hansen, K. Kabin, T. I. Gombosi, M. R. Combi, D. L. DeZeeuw, K. G. Powell, and A. J. Kliore (2001), The interaction between the magnetosphere of Saturn and Titan's ionosphere, *J. Geophys. Res.*, *106*, 6151–6160, doi:10.1029/2000JA000183.

Neubauer, F. M., et al. (2006), Titan's near magnetotail from magnetic field and electron plasma observations and modeling: Cassini flybys TA, TB, and T3, *J. Geophys. Res.*, *111*, A10220, doi:10.1029/2006JA011676.

Roboz, A., and A. F. Nagy, (1994), The energetics of Titan's ionosphere, *J. Geophys. Res.*, *99*(A2), 2087–2093, doi:10.1029/93JA02286.

Schunk, R. W., and A. F. Nagy (2000), Ionospheres: Physics, plasma physics, and chemistry, in Cambridge Atmos. Space Sc. Ser., edited by A. J. Dressler, J. T. Houghton, and M. J. Rycroft, pp. 82–84, Cambridge University Press, Cambridge, U.K.

Sillanpää, I., E. Kallio, P. Janhunen, W. Schmidt, K. Mursula, J. Vilppola, and P. Tanskanen (2006), Hybrid simulation study of ion escape at Titan for different orbital positions, 2006. *Adv. Space Res.*, *38*: 799–805, doi:10.1016/j.asr.2006.01.005.

Strobel, D. F. (2008), Titan's hydrodynamically escaping atmosphere, *Icarus*, *193*, 588–594, doi:10.1016/j.icarus.2007.08.014.

Strobel, D. F. (2009), Titan's hydrodynamically escaping atmosphere: Escape rates and the structure of the exobase region, *Icarus*, in press.

Tanaka, T., and K. Murawski (1997), Three-dimensional MHD simulation of the solar wind interaction with the ionosphere of Venus: Results of two-component reacting plasma simulation, *J. Geophys. Res.*, *102*(A9), 19,805–19,822, doi:10.1029/97JA01474.

Tseng, W.-L., W.-H. Ip, and A. Kopp (2008), Exospheric heating by pickup ions at Titan, *Adv. Space Res.*, *42*, 54–60, doi:10.1016/j.asr.2008.03.009.

Vuitton, V., R. V. Yelle, and M. J. McEwan (2007), Ion chemistry and N-containing molecules in Titan's upper atmosphere, *Icarus*, *191*, 722–742, doi:10.1016/j.icarus.2007.06.023.

Wahlund, J.-E., et al. (2005), Cassini measurements of cold plasma in the Ionosphere of Titan, *Science*, *308*, 986–989, doi:10.1126/science.1109807.

Waite, J. H., et al. (2004), The Cassini Ion and Neutral Mass Spectrometer (INMS) investigation, *Space Sci. Rev.*, *114*, 113–231, doi:10.1007/s11214-004-1408-2.

Waite, J. H., Jr., D. T. Young, T. E. Cravens, A. J. Coates, F. J. Crary, B. Magee, and J. Westlake (2007), The process of tholin formation in Titan'(tm)s upper atmosphere, *Science*, *316*, 870–875, doi:10.1126/science.1139727.

Whitten, R. C., B. Baldwin, W. C. Knudsen, K. L. Miller, and K. Spenner (1982), The Venus ionosphere at grazing incidence of solar radiation: Transport of plasma to the night ionosphere, *Icarus*, *51*, 261–270, doi:10.1016/0019-1035(82)90082-3.

Yelle, R. V., J. Cui, and I. C. F. Müller-Wodarg (2008), Methane escape from Titan's atmosphere, *J. Geophys. Res.*, *113*, E10003, doi:10.1029/2007JE003031.

K. Ågren and J. E. Wahlund, Swedish Institute of Space Physics, Box 537, SE-75121 Uppsala, Sweden.

J. Cui, M. K. Dougherty, and M. Galand, Space and Atmospheric Physics Group, Department of Physics, Imperial College, Prince Consort Road, London SW7 2BW, UK. (j.cui@imperial.ac.uk)

J. H. Waite Jr., Southwest Research Institute, 6220 Culebra Road, San Antonio, TX 78228, USA.

R. V. Yelle, Lunar and Planetary Laboratory, University of Arizona, 1629 East University Boulevard, Tucson, AZ 85721, USA.